Universiteit Leiden
The Netherlands

APEX and NOEMA observations of H2S in nearby luminous galaxies and the ULIRG Mrk 231: a possible relation between dense gas properties and molecular outflows

Sato, M.T.; Aalto, S.; Kohno, K.; König, S.; Harada, N.; Viti, S.; ... ; Gorski, M.

Citation

Sato, M. T., Aalto, S., Kohno, K., König, S., Harada, N., Viti, S., … Gorski, M. (2022). APEX and NOEMA observations of H2S in nearby luminous galaxies and the ULIRG Mrk 231: a possible relation between dense gas properties and molecular outflows. *Astronomy & Astrophysics*, *660*, A82. doi:10.1051/0004-6361/202141260

Version:	Accepted Manuscript
License:	Leiden University Non-exclusive license
Downloaded from:	https://hdl.handle.net/1887/3561945

Note: To cite this publication please use the final published version (if applicable).

Astronomy & Astrophysics manuscript no. H2S_toEditor
March 14, 2022
©ESO 2022

arXiv:2203.05851v1 [astro-ph.GA] 11 Mar 2022

APEX and NOEMA observations of H_2S in nearby luminous galaxies and the ULIRG Mrk 231

Is there a relation between dense gas properties and molecular outflows?

M.T. Sato[1], S. Aalto[1], K. Kohno[2], S. König[1], N. Harada[3], S. Viti[4,5], T. Izumi[3], Y. Nishimura[2,3], and M. Gorski[1]

[1] Department of Space, Earth and Environment, Chalmers University of Technology, Onsala Space Observatory, SE-439 92 Onsala, Sweden
e-mail: mamiko@chalmers.se

[2] Institute of Astronomy, Graduate School of Science, The University of Tokyo, 2-21-1 Osawa, Mitaka, Tokyo 181-0015, Japan

[3] National Astronomical Observatory of Japan, 2-21-1 Osawa, Mitaka, Tokyo 181-8588, Japan

[4] Leiden Observatory, Leiden University, PO Box 9513, 2300 RA, Leiden, The Netherlands

[5] Department of Physics and Astronomy, UCL, Gower Street, London, WC1E 6BT, UK

Received XXX; accepted XXX

ABSTRACT

Context. In order to understand the evolution and feedback of Active Galactic Nuclei (AGN) and star formation it is important to use molecular lines as probes of physical conditions and chemistry.

Aims. We use H_2S to investigate the impact of starburst and AGN activity on the chemistry of the molecular interstellar medium in luminous infrared galaxies. Specifically our aim was to search for evidence of shock-enhancement of H_2S related to galactic-scale mechanical feedback processes such as outflows.

Methods. Using the APEX single dish telescope, we have observed the 1_{10}–1_{01} transition of ortho-H_2S at 168 GHz towards the centres of twelve nearby luminous infrared galaxies. We have also observed the same line towards the ultra luminous infrared galaxy (ULIRG) Mrk 231 with the NOEMA interferometer.

Results. We have detected H_2S towards NGC 253, NGC 1068, NGC 3256, NGC 4418, NGC 4826, NGC 4945, Circinus, M 83 and Mrk 231. Upper limits were obtained for NGC 1097, NGC 1377 and IC 860. We also detected line emission from HCN 2–1 in all galaxies in the APEX survey, and HCO^+, HNC, CH_3CN, CH_3OH, H_2CS, HOC^+ and SO in several of the sample galaxies. Mrk 231 has a rich 2 mm molecular spectrum and, apart from H_2S, we detect emission from HC_3N, CH_3OH, $HC^{18}O^+$, C_2S and CH_3CCH. Four galaxies show elevated H_2S emission relative to HCN: Circinus, NGC 3256, NGC 4826 and NGC 4418. We suggest that the high line ratios are caused by elevated H_2S abundances in the dense gas. However, we do not find any clear connection between the H_2S/HCN line intensity ratio, and the presence (or speed) of molecular outflows in the sample galaxies. Therefore H_2S abundances do not seem to be globally affected by the large-scale outflows. In addition, the H_2S/HCN line ratio is not enhanced in the line wings compared to the line core in Mrk 231. This suggests that H_2S abundances are not increased in the dense gas in the outflow. However, we do find that the H_2S and HCN luminosities (L_{H_2S} and L_{HCN}) correlate well with the total molecular gas mass in the outflow, $M_{outflow}(H_2)$, in contrast to L_{CO} and L_{HCO^+}. We also find that the line luminosity of H_2S correlates with total infrared luminosity in a similar way that H_2O does.

Conclusions. We do not find any evidence of H_2S abundance enhancements in the dense gas due to galactic-scale outflows in our sample galaxies, or in the high-resolution study of Mrk 231. We discuss possible mechanisms behind the suggested H_2S abundance enhancements in NGC 4418, Circinus, NGC 3256 and NGC 4826. These include radiative processes (for example X-rays or cosmic-rays) or smaller scale shocks. Further high resolution, and multi-transition studies are required to determine the cause behind the elevated H_2S emission in these galaxies. We suggest that L_{H_2S} serves as a tracer of the dense gas content, similar to L_{HCN}, and that the correlation between L_{H_2S} and $M_{outflow}(H_2)$ implies a relation between the dense gas reservoir and the properties and evolution of the molecular feedback. This potential link requires further study since it holds important keys to our understanding of how the properties of molecular outflows relate to that of their host galaxies. Finally, the similar IR-correlation coefficients between H_2S and H_2O may indicate that they originate in the same regions in the galaxy: warm gas in shocks or irradiated by star formation or an AGN.

Key words. galaxies: evolution – galaxies: nuclei – galaxies: ISM – ISM: molecules – ISM: jet and outflows

1. Introduction

Molecular gas plays an important role in the bursts of star formation and feeding of Super Massive Black Holes (SMBHs), in particular when collisions of gas-rich galaxies funnel massive amounts of material into nuclei of luminous and ultra luminous infrared galaxies (LIRGs/ULIRGs) (Sanders & Mirabel 1996; Iono et al. 2009). Molecular gas probes important physical processes such as massive outflows powered by the nuclear activity (e.g. Sturm et al. 2011; Feruglio et al. 2011; Chung et al. 2011;

Table 1: Basic information of sources

Galaxy	α (J 2000) (h:m:s)	δ (J 2000) (° : ′ : ″)	D^a (Mpc)	$L_{\rm IR}{}^b$ ($L_\odot$)	type	Outflow^c	Water vapor^d	$t_{\rm int}{}^e$ (hours)	rms[LSB/USB]^f (mK)
NGC 253	00:47:33.1	−25:17:18	3.1	3.0×10^{10}	SB	Yes$^{(1)}$	No	1.5	0.48/0.87
NGC 1068	02:42:40.7	−00:00:48	13.7	2.0×10^{11}	AGN+SB	Yes$^{(2)}$	No	3.5	0.35/0.60
NGC 1097	02:46:19.0	−30:16:30	16.8	5.0×10^{10}	LLAGN	No	No	1.2	0.30/0.51
NGC 1377	03:36:39.1	−20:54:08	23.66	1.3×10^{10}	AGN?	Yes$^{(3)}$	No	7.7	0.24/0.60
NGC 3256	10:27:51.3	−43:54:13	35.35	3.6×10^{11}	SB	Yes$^{(4)}$	Yes$^{(1)}$	6.9	0.20/0.38
NGC 4418	12:26:54.6	−00:52:39	31.9	1.0×10^{11}	AGN	Yes$^{(5)}$	Yes$^{(2)}$	1.1	0.41/0.67
Mrk 231	12:56:14.2	+56:52:25	171.8	3.2×10^{12}	AGN+SB	Yes$^{(6)}$	Yes$^{(3)}$		0.6(mJy/beam)/ -
NGC 4826	12:56:43.6	+21:40:59	3.1	4.0×10^{9}	AGN	No	No	2.8	0.27/0.66
NGC 4945	13:05:27.5	−49:28:06	3.9	3.0×10^{10}	AGN/SB	Yes$^{(7)}$	No	4.9	0.46/1.0
IC 860	13:15:03.5	+24:37:08	59.1	1.5×10^{11}	LIRG	Yes$^{(8)}$	Yes$^{(4)}$	2.6	0.52/0.80
NGC 5128	13:25:27.6	−43:01:09	4.0	2.0×10^{11}	AGN	Yes$^{(9)}$	No	1.4	- / -
M 83	13:37:00.9	−29:51:56	3.6	1.0×10^{10}	SB	No	No	1.4	0.51/0.96
Circinus	14:13:09.9	−65:20:21	4.2	6.9×10^{10}	AGN/SB	Yes$^{(10)}$	No	3.5	0.37/0.81

Notes. Note.
$^{(a)}$ Distances taken from Sanders et al. (2003) except for Circinus which value was taken from the NASA/IPAC Extragalactic Database; $^{(b)}$ infrared luminosities taken from Sanders et al. (2003) except for Circinus which was calculated from the flux densities of 12μm, 25μm,60μm and 100μm taken from Brauher et al. (2008, Table 1); $^{(c)}$ Presence of molecular outflow report. (1) e.g. Bolatto et al. (2013a); Walter et al. (2017), (2) e.g. Emsellem et al. (2006); Barbosa et al. (2014); García-Burillo et al. (2015),(3) e.g. Aalto et al. (2012, 2016),(4) e.g. Sakamoto et al. (2014); Michiyama et al. (2018), (5) e.g. Ohyama et al. (2019), (6) e.g. Spoon et al. (2013) , (7) Henkel et al. (2018), (8) e.g. Aalto et al. (2019) (9) e.g. Israel et al. (2017), (10) Curran et al. (1999); Zschaechner et al. (2016); $^{(d)}$ Presence of water detection. (1) Herschel SPIRE data, (2) González-Alfonso et al. (2012), and Herschel SPIRE data ,(3) González-Alfonso et al. (2010),(4) Herschel PACS data ; $^{(e)}$ On source observation time ; $^{(f)}$ Noise level obtained from the CLASS (http://www.iram.fr/IRAMFR/GILDAS).

Aalto 2012; Aalto et al. 2012; Cicone et al. 2014; Sakamoto et al. 2014; Aalto et al. 2015a; Fluetsch et al. 2019; Veilleux et al. 2020). These outflows help to regulate the growth of galaxy nuclei and the implied outflow momenta suggest that the inner regions of these galaxies may be cleared of material within a few Myr (e.g. Feruglio et al. 2011; Cicone et al. 2014). The morphology of the molecular feedback ranges from wide-angle winds (Veilleux et al. 2013), gas entrained by radio jets (Morganti et al. 2015; García-Burillo et al. 2015; Dasyra et al. 2016) to collimated molecular outflows (Aalto et al. 2016; Sakamoto et al. 2017; Barcos-Muñoz et al. 2018; Falstad et al. 2019).

The fate of the molecular gas is still not well understood. One question is whether the gas is expelled from the galaxy or it returns to fuel another cycle of activity (e.g. Pereira-Santaella et al. 2018; Lutz et al. 2020). It is also not known if the molecular clouds are being swept up from a circumnuclear disk or formed in the outflow (e.g. Ferrara & Scannapieco 2016). Another question is whether the clouds expand and evaporate or if they condense and form stars in the outflow (Maiolino et al. 2017). A detailed study of the physical conditions of the molecular gas in outflows is necessary to understand its origin, how it evolves within the outflow, as well as how this is linked to the nature of the driving force.

Important extragalactic probes of cloud properties include molecules such as HCN, HCO^+, HNC, CN and HC_3N. These molecules have high dipole moments which means that they normally require high densities ($n > 10^4$ cm^{-3}) for efficient excitation. Hence they are in general more tightly related to dense star-forming gas compared to low-J transitions of CO, as shown by Gao & Solomon (2004).

The detection of luminous HCN and CN emission in, often AGN-powered, molecular outflows is evidence of the presence of large amounts of dense molecular gas (e.g. Aalto 2012; Sakamoto et al. 2014; Matsushita et al. 2015; García-Burillo et al. 2015; Privon et al. 2015; Cicone et al. 2020). (Although we should note that faint, but widespread, HCN emission may also emerge from more diffuse gas (e.g. Nishimura et al. 2017).)

To understand the origin of the dense gas in outflows, we require tracers that probe specific physical and chemical conditions. One of the most reactive elements is sulphur: its chemistry is very sensitive to the thermal and kinetic properties of the gas. Sulphur-bearing molecules, such as H_2S, SO and SO_2, appear to be unusually abundant in clouds with high mass star formation, accompanied by shock waves and/or high temperatures (e.g. Mitchell 1984; Minh et al. 1990). Hence observations of sulphur-bearing molecules could be used to constrain the properties of the dense gas in outflows.

H_2S is often assumed to be the most abundant sulphur-bearing species on ice mantles, as hydrogenation of sulphur should be very efficient on the dust grains, despite not being detected in interstellar ices (Charnley 1997; Wakelam et al. 2004; Viti et al. 2004). In quiescent star-forming regions, gas-phase abundances of H_2S are therefore low because they are depleted on grains.

Strong shocks can sputter H_2S off the grains moving into the gas phase. There are many theoretical studies to test this hypothesis (e.g. Woods et al. 2015), giving ample evidence of enhanced gas phase H_2S in warm and/or shocked environments. In model calculations, Holdship et al. (2017) have shown that as a C-type shock passes through the cloud, sulphur is first transformed into H_2S and its abundance increases greatly in the post-shock gas. H_2S chemistry and grain-processing features share several properties with that of water, H_2O, but with the added advantage that its ground state transition occurs at a wavelength of λ=2 mm and can be observed with ground-based telescopes.

H_2S seems to be a promising tracer to probe outflows and nuclear, dusty activity in galaxies. Photon Dominated Regions (PDRs) may also contribute significantly to the H_2S emission

(e.g. Goicoechea et al. 2021). Here we present the results of an Atacama Pathfinder Experiment (APEX) single dish telescope pilot survey of the 168.7 GHz $1_{1,0}$–$1_{0,1}$ transition of H_2S toward a sample of galaxies to study the relationship between H_2S emission and the outflow activity of the galaxies. We also present 168.7 GHz IRAM Northern Extended Millimiter Array (NOEMA) H_2S observations of the nucleus and outflow of the ULIRG merger Mrk 231.

The paper is organised as follows. In Sec. 2 we present the galaxy sample, as well as the APEX and NOEMA observation, and in Sec. 3 the results. In Sec. 4 we discuss the luminosity of the H_2S emission in relation to that of other tracers such as HCN, HNC, HCO^+, H_2O and CH_3CN and also in relation to the presence of an outflow. In Sec. 5 we present our conclusions and an outlook.

Table 2: List of molecular lines in the APEX band

Molecule	Transition	Rest Frequency (GHz)	Sideband
CH_3OH	1_1–1_0	165.050	LSB
CH_3CN	9–8	165.569	LSB
H_2S	$1_{1,0}$–$1_{0,1}$	168.763	LSB
H_2CS	5–4	169.113	LSB
HCN	2–1	177.261	USB
HCO^+	2–1	178.375	USB
SO	10_{10}–11_{10}	178.615	USB
HOC^+	2–1	178.972	USB
HNC	2–1	181.324	USB

2. Observations

2.1. The sample

In Table 1 the sources, consisting of a total of 13 (12 are observed with APEX and one with NOEMA) galaxies, are presented. They were selected as a mixture of starburst- and AGN-powered luminous infrared galaxies, which are observable with APEX. Some have detected molecular outflows while other have no indications of outflows (Table 1). The objects are nearby ($D < 60$ Mpc) to allow us to detect H_2S emission with a single dish telescope. The Mrk 231 observations stem from a separate NOEMA observational program that is included in this paper since it fits with the observational goals of the APEX program. Mrk 231 is more distant than the objects observed with APEX.

2.2. APEX SEPIA B5

The observations were carried out with APEX SEPIA Band 5 under program codes 096.F-9331(A), 099.F-9312(A) and 0100.F-9311(A). NGC 4945, Circinus, NGC 3256, NGC 1377 and IC 860 were observed in September and November 2015. NGC 1068, NGC 253, NGC 4418, M 83, NGC 4826, NGC 5128 and NGC 1097 were observed in June and August 2017. The basic information of the sources and the observational details are listed in Table 1 and Table 2, respectively. The heterodyne SEPIA band 5 receiver, which covers the frequency range from 159 to 211 GHz, was used as a frontend. In the backend we used the PI-XFFTS spectrometer, which consists of two units that provide a bandwidth of 4 GHz and 32,768 spectral channels each. The observations were done in the position-switching mode in the frequency ranges 165-169 GHz and 177-181 GHz which allowed for a simultaneous search for emission lines of e.g., H_2S, HCN and HCO^+. The typical precipitable water vapor level during the observations was ~1-2 mm. The temperature scale of the data is in units of the antenna temperature corrected for the atmospheric attenuation, T'_A. The full width at half maximum (FWHM) of the sidebands of the telescope can be computed approximately as $FWHM_{LSB}$=37.″4 × (167/[ν_{obs}/GHz]) and $FWHM_{USB}$=34.″9 × (179/[ν_{obs}/GHz]), respectively, where ν_{obs} is the observed frequency.

CLASS[1] was used for further analysis including baseline subtraction of a polynomial of order 1 for individual scans and spectral smoothing. The native channel widths of the observations ranged from 0.07 km s^{-1} for USB to 0.14 km s^{-1} for LSB. The data were smoothed to a final velocity resolution of 50 km s^{-1}.

2.3. NOEMA observations

Observations of Mrk 231 were carried out with the NOEMA on April 21, 2017. Data were obtained with eight antennas in the most compact configuration, with baselines between 24 and 176 m. The phase centre of the observations was located at α=12:56:14.2 and δ=+56:52:25. The 2 mm-band receivers were tuned to 161.934 GHz to cover the H_2S 1_{10} − 1_{01} line in the 3.6 GHz bandwidth of WideX. The instrumental spectral resolution was 1.95 MHz (~3.6 km s^{-1}). For analysis purposes we smoothed the data to ~20 MHz channel spacing (~37.0 km s^{-1}), resulting in 1σ rms noise levels per channel of ~0.6 mJy beam^{-1}. During the observations, different sources were observed for calibration purposes: MWC 349 as flux calibrator, 3C 454.3 as bandpass calibrator, and J1418+546 and J1300+580 as phase calibrators.

Data reduction and analysis were performed using the CLIC and MAPPING software packages within GILDAS[2], and AIPS[3]. Applying a natural weighting scheme led to a beam size of 2.91″ × 2.13″, with position angle 75.64°.

3. Results

3.1. APEX

Several molecular lines are detected towards the targeted galaxies (see Table 2). Of the 12 galaxies in the APEX sample, 11 were detected in HCN and HCO^+ 2–1, and nine galaxies were detected in the target H_2S line. In addition, we also detected eight galaxies in SO, seven in HNC and CH_3OH, four in CH_3CN, H_2CS and HOC^+. Spectra are shown in Fig. A. The integrated line intensities are presented in Table B.

3.2. NOEMA - Mrk 231

Fig. 1 shows the full bandwidth NOEMA spectrum of Mrk 231. We have labelled all molecular lines that are brighter than 3σ above noise level and they are also listed in Table 3. H_2S is clearly detected with a peak intensity of ~7 mJy. The $HC^{18}O^+$ 2–1 line is also bright with a peak intensity almost comparable to that of H_2S. H_2CS 5-4, which is also detected in NGC 4945,

[1] See http://www.iram.fr/IRAMFR/GILDAS for more information about the GILDAS software.

[2] http://www.iram.fr/IRAMFR/GILDAS

[3] http://www.aips.nrao.edu/index.shtml

Table 3: List of molecular lines in the NOEMA band (Mrk 231)

Molecule	Transition	Rest Frequency (GHz)
HC_5N	63–62	167.718
$CH_3OH^{\dagger}$	9_1–9_0	167.931
CH_3OH	v_2=2, 10^+_8– 11^+_5	168.076
$CH_3OH^{\dagger}$	40_3–39_5	168.296
C_2S	13_{13}–12_{12}	168.407
H_2S	$1_{1,0}$–$1_{0,1}$	168.763
H_2CS	5–4	169.113
CH_3OH	10_1–10_0	169.335
CH_3OH	15_1–14_3	169.488
$C_2S^{\diamond}$	13_{14}–12_{13}	169.753
CH_3OH	3_2–2_1	170.060
$HC^{18}O^+$	2–1	170.323
CH_3CCH	10–9	170.876

Notes. † A possible alternative identification here is $H_2^{34}S$.$^{\diamond}$Alternative identifications are NH_2CN or ^{34}SOH.

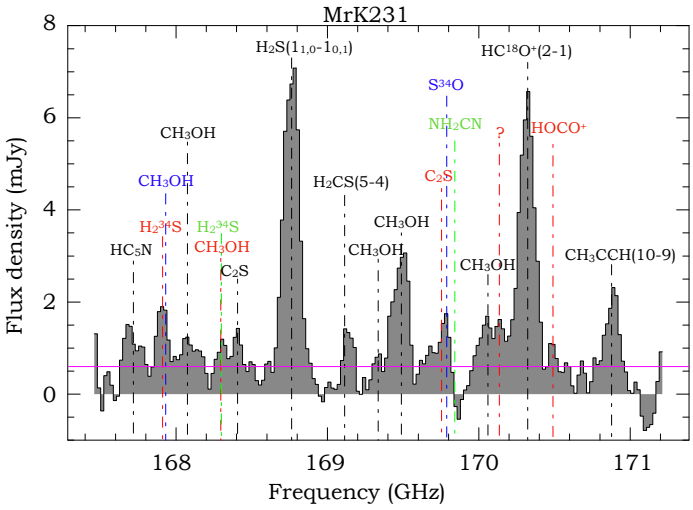

Fig. 1: NOEMA broad-band (3.6 GHz), 2mm spectrum of Mrk 231, centred on H_2S. The x-axis is rest frequency and the y-axis is flux in mJy. Identified lines have detection thresholds above 3σ (rms, indicated in the magenta line).

NGC 4418, NGC 253 and NGC 1068 with APEX, shows a tentative detection. In Fig. 2 we show a spectrum zoomed in on the H_2S line in Mrk 231. It shows that H_2S is detected in the line wings up to velocities of -300 km s^{-1} on the blueshifted side and possibly out to 500 km s^{-1} on the redshifted side. The integrated line intensity of H_2S is presented in Table4.

4. Discussion

This is the first survey of the λ=2 mm 1_{10}–1_{01} line of o-H_2S in luminous infrared galaxies. In this paper we report eight new detections, seven with APEX and one from NOEMA observations. To date, only three detections of 2 mm H_2S line emission have been reported outside our own galaxy : Large Magellanic Cloud (LMC) (e.g. Heikkilä et al. 1999), NGC 253 (e.g. Martin et al. 2005) and Arp 220 (e.g. Martín et al. 2011). Our sample, which

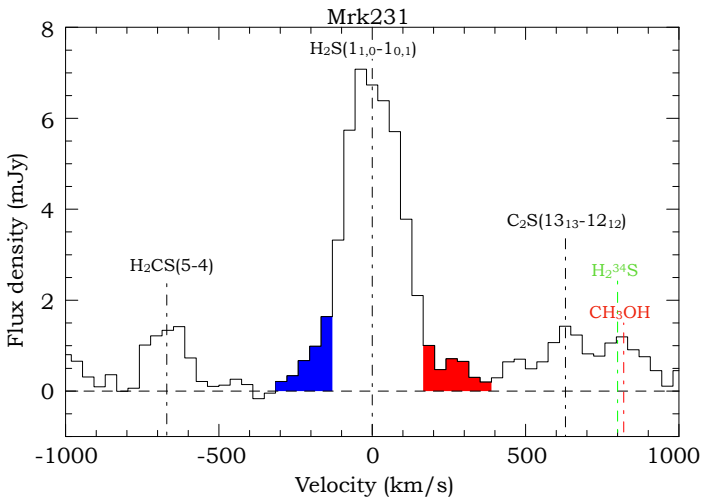

Fig. 2: NOEMA H_2S spectrum of Mrk 231 (zoomed in from Fig.1). The x-axis is in km/s relative to the central velocity (12642 km/s). Red- and blue-shifted line-wing emission is indicated with corresponding colours. Other identified lines are indicated in the figure (same as in Fig.1)

is chosen from nearby LIRGs (see Sec. 2.1), includes a variety of galaxies in terms of morphology and kinematics.

4.1. H_2S formation mechanisms

H_2S can be formed through hydrogenation of a sulphur atom on grain surfaces, which can then be either i) thermally desorbed by shocks (Esplugues et al. 2014, Fig. 2) or by IR radiation (e.g. Crockett et al. 2014), ii) photodesorbed by UV radiation, iii) desorbed after cosmic ray impacts, and iv) sputtered by shocks. Chemical desorption could be also efficient to release H_2S into the gas phase (e.g. Oba et al. 2019; Navarro-Almaida et al. 2020), but it is not a dominant mechanism when we focus on starburst and AGN-host galaxies. Hydrogenation of sulphur is also possible in the gas-phase if the kinetic temperature is higher than a few to several 1000 K (Mitchell 1984). For gas densities in excess of n=10^4 cm^{-3}, gas and dust are coupled and thermalised with similar temperatures. Therefore, under the assumption that most of the H_2S emission is emerging from dense gas, which kinetic temperature can be between 10 to 300 K, hydrogenation in the gas-phase is unlikely because it is unlikely that the bulk of the dense gas can be maintained at such a high temperature. On smaller scales, close to heating sources, such high temperatures are however possible.

4.1.1. H_2S enhancement via shocks

Shocks can cause both thermal desorption and mantle sputtering. For the case where the sulphur species are sputtered into the gas-phase by strong shocks, Fig.3 shows the average fractional abundance as a function of shock velocity for H_2S (Holdship et al. 2017). In this figure, it can be seen that for low pre-shock gas densities (10^3 cm^{-3}), the fractional abundance is 10^{-8} for shock velocities less than 20 km s^{-1}, and increases by a factor of ~100 for shock velocities >30 km s^{-1}. For higher pre-shock gas densities (>10^4 cm^{-3}), the abundance reaches values ~10^{-6} even for shock velocities as low as ~5 km s^{-1}. This suggests that a high abundance of this molecule could be due to the passage of

Table 4: NOEMA observation result for Mrk 231

Species	Transition	Line peak ($T_{A,peak}$) (mJy beam^{-1})	Core I^a (Jy kms^{-1})	Δv (kms^{-1})	Wings $I_{redwing}{}^b$ (Jy kms^{-1})	$I_{bluewing}{}^c$ (Jy kms^{-1})
H_2S	$1_{1,0}$–$1_{0,1}$	7.08	1.69±0.11	224.68±29.48	0.07±0.07	0.02±0.07
HCN	J=2–1	90.6	24.09±0.14	255	1.74±0.14	1.18±0.14
HCO^+	J=2–1	68.0	15.58±0.14	215	0.78±0.14	1.09±0.14

Notes. The values for HCN and HCO^+ are taken from Lindberg et al. (2016). (a) Integrated intensity between -250 and 250 km s^{-1}. (b) Integrated intensity between 350 and 515 km s^{-1} for H_2S, between 350 and 990 km s^{-1} for HCN and HCO^+. (c) Integrated intensity between -538 and -350 km s^{-1} for H_2S, between -990 and-350 km s^{-1} for HCN and HCO^+.

Table 5: Integrated intensity ratios

Source	$R_{\frac{HCN}{HCO^+}}$	$R_{\frac{H_2S}{HCN}}$	$R_{\frac{H_2S}{HCO^+}}$	$R_{\frac{CH_3OH}{HCN}}$	$R_{\frac{CH_3CN}{HCN}}$	$R_{\frac{SO}{HCN}}$
from APEX observations						
NGC 3256	0.54±0.11	0.12±0.03	0.07±0.01	>0.03±0.01	<0.01±0.01	0.06±0.02
NGC 1068	1.39±0.30	0.05±0.01	0.08±0.02	>0.02±0.01	<0.02±0.01	0.02±0.01
IC 860	>6.31±6.39	<0.10±0.11	<0.620.93±	<0.07±0.09	0.48±0.13	<0.16±0.16
NGC 4418	1.73±0.37	0.17±0.08	0.30±0.14	—	0.19±0.08	0.12±0.05
Circinus	0.86±0.18	0.13±0.03	0.11±0.02	>0.03±0.01	<0.01±0.01	0.03±0.01
NGC 1097	1.21±0.26	0.05±0.02	0.06±0.02	>0.02±0.02	<0.02±0.02	<0.02±0.02
NGC 4945	1.04±0.22	0.05±0.01	0.05±0.01	>0.06±0.01	0.03±0.01	<0.01±0.01
NGC 253	0.99±0.21	0.09±0.02	0.09±0.02	>0.06±0.01	0.03±0.01	0.03±0.01
M 83	0.94±0.20	0.08±0.02	0.07±0.02	>0.07±0.02	<0.02±0.01	<0.03±0.03
NGC 4826	1.12±0.24	0.18±0.04	0.20±0.04	<0.03±0.03	<0.03±0.03	<0.06±0.07
from NOEMA observations						
Mrk 231 (Core)	1.55	0.07	0.11	—	—	—
(B.wing)	1.08	0.02	0.02	—	—	—
(R.wing)	2.23	0.04	0.09	—	—	—

Notes. The line intensity ratio of two molecular lines, $R_{line1/line2}$ from APEX and NOEMA observations. Transitions of the lines are: HCN 2-1, HCO^+ 2-1, H_2S $1_{1,0} - 1_{0,1}$, CH_3OH $1_1 - 1_0$, CH_3CN 9-8, and SO $10_{10} - 11_{10}$. The values for the blue and red wings for Mrk 231 are calculated using the integrated intensities between the same velocity ranges as in Table 4.

a shock in the absence of other mechanisms capable of releasing H_2S from the ices. The caveat here is that this model considers only the case when most of the sulphur hydrogenates on the grains.

According to chemical models, H_2S transforms quickly into SO, SO_2, etc., within a timescale of $\leq 10^4$ yr (e.g. Pineau des Forets et al. 1993). Shock elevation of H_2S abundances therefore requires continuous replenishment, for example by internal shocks in the outflow. Internal shocks can occur if the molecular gas is interacting with hotter material in the outflow or if parts of the outflow is interacting with slower/faster moving gas components, for example due to periodic ejection processes. It is also possible that H_2S is enhanced in highly turbulent gas. If so, the link to the outflow activity becomes less clear and may depend on whether the outflow process is feeding turbulence in the gas in a fountain scenario (e.g. Aalto et al. 2020). Other sources that drive turbulence include accretion and inflow, galactic rotation and stellar feedback (Klessen & Glover 2016).

4.1.2. H_2S enhancement via thermal desorption, uv radiation and cosmic rays

As discussed above, other possible method for getting H_2S off the grains and into the gas-phase is by thermal desorption from warm grains, non-thermal UV photo-desorption, and cosmic-ray-induced desorption. In a recent Herschel study of higher rotationally excited H_2S lines in Orion hot core, Crockett et al. (2014) pointed to an H_2S origin in dense, embedded gas, in close proximity to a hidden self-luminous protostellar source (i.e. heating the grains above the H_2S sublimation temperature). In addition, Goicoechea et al. (2021) discussed and modelled the photodesorption of H_2S in UV-illuminated environment (PDRs) and this is a possible additional H_2S formation mechanism for some of the sample galaxies. However, for some objects the gas and dust column densities will be too high to allow the UV radiation to penetrate very far. A further possible mechanism is cosmic-ray-induced desorption. These scenarios are further discussed in Sec. 4.4.

4.2. Column density and abundance

In this section we make simple estimates of column densities and abundances for basic comparisons with other sources and shock

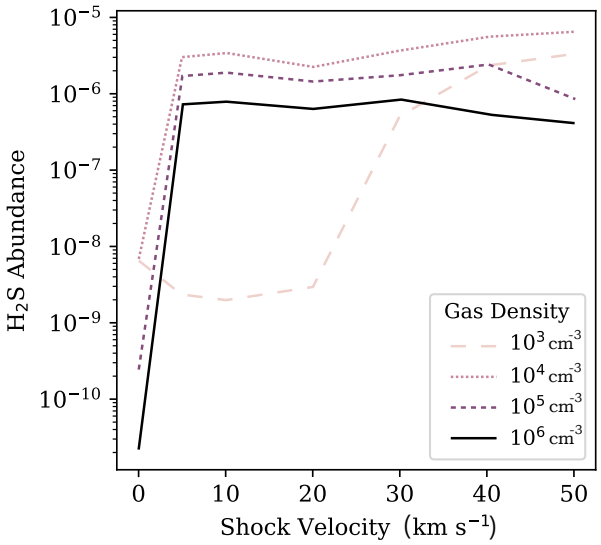

Fig. 3: Average fractional abundance as a function of shock velocity for H_2S from Holdship et al. (2017). Each line shows a different pre-shock density; the log(n_H) values are given in the lower right plot.

models. We assume collisional excitation for the H_2S molecule throughout the paper (e.g. Mangum & Shirley 2015)[4]. H_2S may also be pumped by infrared radiation, but Crockett et al. (2014) argued that IR pumping for the transitions of H_2S lower than J=3 is unlikely because these transitions occur at longer wavelengths ($\lambda > 100\mu m$).

Column densities of H_2S, HCN and HCO^+ molecules for each galaxy were calculated using the formalism in Mangum & Shirley (2015, 2016, 2017). Since we have no direct information on the excitation of the H_2S molecule nor the distribution of its emission, we have to make some assumptions to estimate the column densities. We have to assume an excitation temperature, T_{ex}, and we estimated column densities for three different values of T_{ex} of 30 K, 60 K and 150 K to compare the results. This range of temperature is reflecting the span of kinetic temperature typically found in the inner regions of galaxies (e.g. Aalto et al. 1995; Mangum et al. 2013, 2019; Salak et al. 2014). This is often an upper limit to the excitation temperature. We also assumed a beam-filling factor of unity f_s=1 and optically thin ($\tau << 1$) emission for all lines for simplicity. We compare the H_2S to the HCN abundance, assuming that both lines emerge from the same dense gas component and have the same T_{ex} (see Sec.4.2.1 for a discussion of caveats). The effect of these simplifying assumptions are to some extent cancelled out when we use the same assumption for all species and compare their ratios. For example, we find that the difference between resulting column density ratios for different T_{ex} is small, less than a factor of 2.

We consider the two most extreme cases in the observed H_2S/HCN line ratios: NGC 4418 and NGC 1097 (see Table 5). We estimate the H_2S/HCN abundance ratio (=column density ratio) to be $X(H_2S/HCN)$~0.1 for NGC 4418 and ~0.03 for NGC 1097 (for T_{ex}=60 K). We choose the column density values derived for an T_{ex} of 60 K since it is an intermediate value for T_{ex}. As note above, the impact of the T_{ex} on the column density ratio is quite small.

[4] $n_{crit,H_2S} \approx 7.8 \times 10^5$[cm^{-3}], $n_{crit,HCN(2-1)} \approx 1.3 \times 10^7$[cm^{-3}], $n_{crit,HCO^+(2-1)} \approx 1.2 \times 10^6$[cm^{-3}] and $n_{crit,CO(1-0)} \approx 2.2 \times 10^3$[cm^{-3}] at T_k=30 K.See Appendix C.

The difference in abundance ratio reflects quite well the difference in line intensity ratio between the two galaxies. We will therefore use the integrated intensity of H_2S relative to HCN and HCO^+ in Sections 4.3 and 4.4 to indicate potential H_2S enhancements in relation to the dense gas. The estimated values of $X(H_2S/HCN)$ seem reasonable compared to those found for the Galactic Orion star forming complex. The value for $X(H_2S/HCN)$ varies strongly within the region, from $< 10^{-4}$ in the ridge (quiescent gas) to ~0.3 for the plateau (shocked gas) (Blake et al. 1987) while the $X(H_2S/HCN)$ for the Orion hot core may be greater than unity.

We also determined the H_2S abundance in relation to H_2 to $X(H_2S) \approx 1.3 \times 10^{-7}$ and $X(H_2S) \approx 1.7 \times 10^{-8}$ for NGC 4418 and NGC 1097, respectively. To obtain a value for $N(H_2)$, we obtained the molecular mass from the CO 1–0 luminosity[5] assuming a standard CO-to-H_2 conversion factor (Bolatto et al. 2013b). Assuming that the molecular mass was uniformly distributed in the APEX beam for our H_2S observations we could calculate an average $N(H_2)$. Comparing to the shock model results presented in Fig.3 shows that our simple estimation for $X(H_2S)$ is consistent with a shock origin of the observed H_2S for NGC 4418. On the other hand, Crockett et al. (2014) show that these enhanced H_2S abundances are caused by strong dust heating and subsequent thermal desorption in hot cores. In Sections 4.3 and 4.4 we compare line ratios with dynamical and radiative properties of the galaxies to see if we can determine if outflows may be the cause behind H_2S enhancements in LIRGs.

4.2.1. Caveats

Our column density values are strongly affected by the assumptions on beam-filling factors and T_{ex}. They give average values at best which is acceptable in searching for trends and correlations, but *further high resolution and multi-transition follow-up studies are required to chart the underlying causes behind H_2S intensity enhancements.* One example to illustrate this is NGC 4418. Costagliola et al. (2015) studied the molecular excitation temperatures and column densities of many species in NGC 4418 with high resolution and multi-transition observations using ALMA. They could compensate for the high optical depth of the HCN lines with a population diagram analysis, and (with an optically thin assumption for H_2S) estimated $X(H_2S/HCN)$~0.5. Should we use their LTE values, uncorrected for opacity, then we would arrive at $X(H_2S/HCN)$> 60. The discrepancy of this latter value compared to our result is that Costagliola et al. (2015) use a T_{ex} of 7 K for HCN and 70 K for H_2S while we use the same value for both lines. HCN may exist also in more extended and colder region compared to H_2S, which contribute to lowering the excitation.

4.3. Testing the notion of shock-enhanced H_2S

Out of the 13 sample LIRGs, 10 have been reported to have molecular outflows (See Table1). In Sec. 4.1.1 we discussed a possible link between H_2S enhancement and shocks in galaxies, for example caused by large scale outflows. The sample galaxies display a range in outflow velocity, from slow (150 km s^{-1}) to fast (>250 km s^{-1}).

To search for evidence of elevated H_2S emission related to shock events, we put together line intensity ratios of H_2S/HCO^+

[5] CO 1–0 luminosities taken from Sanders et al. (1991) for NGC 4418 and Gerin et al. (1988) for NGC 1097.

and H_2S/HCN from our observation by APEX and NOEMA (see Table 5)(see discussion in Sec. 4.2).

4.3.1. APEX single dish data

We identify four galaxies with particularly elevated (a factor of two to three higher than in the rest of the sample) H_2S/HCN ratios: Circinus, NGC 3256, NGC 4826 and NGC 4418. Of these, NGC 3256 has a fast molecular outflow (>250 km s^{-1}), Circinus and NGC 4418 have slow outflows (≈150 km s^{-1}) while NGC 4826 has no report of a molecular outflow. Another example is the Seyfert galaxy NGC 1068, which has a striking AGN-driven molecular outflow (e.g. García-Burillo et al. 2014), but has a lower H_2S/HCN ratio compared to NGC 4826, or M83 that lack known molecular outflows. In addition, both NGC 4945 and NGC 253 have slow molecular outflows with velocities of 50 km s^{-1}, but their H_2S line luminosity relative to HCN is quite different from each other (Table 5).

We find that the line ratios show considerable variation among our sample galaxies, but there is no apparent indication that H_2S is more abundant in the galaxies with outflows, nor can we find any link to the outflow velocity. The lack of a clear link between the H_2S/HCO^+ and H_2S/HCN line ratios and the presence, and properties, of an outflow could be because the link is not there, or because the large APEX beam (multi-kpc scale) includes too much extended gas that is unconnected to the outflow. Indeed, H_2S absorption has been detected even in diffuse clouds (Lucas & Liszt 2002) which may also contribute and dilute our results. Furthermore, the single dish data lack the sensitivity and stability necessary to compare the relative H_2S enhancement in the line core to that in the line wings.

Therefore it is important to investigate potential enhancements of H_2S in outflows with high resolution observations, both spectroscopically and spatially, for a sample of galaxies.

4.3.2. Mrk 231 with NOEMA

To search for indications of shock-chemistry in an outflow with higher spatial resolution, we observed the 168 GHz ground state H_2S line with the NOEMA telescope toward Mrk 231.

The ULIRG quasar Mrk 231 has an extremely strong and fast molecular outflow where CO has been detected out to velocities of 750 km s^{-1} (Feruglio et al. 2010). The molecular outflow also shows remarkably luminous HCN emission which is suggested to be caused by large masses of dense molecular gas, but also by elevated HCN abundances (Aalto 2012; Aalto et al. 2015b). It is suggested that the HCN enhancement is caused by the molecular gas being compressed and fragmented by shocks in the outflow.

We detected the H_2S line with a peak intensity of ≈7.2 mJy (Fig. 2) and the line has wings at both sides indicating H_2S emission in the outflow at least out to velocities of -300 kms^{-1} and +500 kms^{-1} (see Sec. 3.2). However, when we compare the relative intensity of the H_2S emission to that of HCN 2–1, we see no sign of an elevated H_2S intensity in the line wings with respect to the core. Therefore, the relatively faint H_2S emission appears inconsistent with the notion of dominant shock-chemistry in the molecular outflow of Mrk 231. More studies of the molecular formation and destruction processes of the Mrk 231 are necessary (See for example the recent detection of CN in the outflow by Cicone et al. (2020)).

It is interesting to compare Mrk 231 to the H_2S-luminous merger LIRG NGC 3256. This galaxy exhibits two strong and fast outflows: one from each nucleus (e.g. Sakamoto et al. 2014). NGC 3256 has a distinct H_2S enhancement in relation to HCN and we require high resolution observations to determine if the enhancement is linked to any, or both, of the two outflows, or to some other part of its molecular emission.

4.4. H_2S enhancement caused by thermal desorption: The "Hot Core"-like nuclear obscuration of NGC 4418

H_2S enhancements may also be caused by other processes such as thermal desorption (see Sec. 4.1.2). For example, in a high resolution study of H_2S towards NGC 253, Minh et al. (2007) argue that H_2S enhancements might be associated with young massive star formation, which may imply a scenario of radiative thermal desorption.

NGC 4418 and IC 860 are suggested to host so called Compact Obscured Nuclei (CONs) in their central regions (e.g. Costagliola et al. 2011, 2013; Sakamoto et al. 2013; Falstad et al. 2019; Aalto et al. 2019). A CON is a region of exceptionally high H_2 column density ($N(H_2)$> 10^{25} cm^{-2}) and with very high IR luminosity surface brightness and gas temperatures (in excess of 200 K). Studies of IC 860 also find that the gas densities can be high with n~10^7 cm^{-3} (Aalto et al. 2019).

Methyl cyanide CH_3CN, known as a tracer of dense and warm gas (e.g. Churchwell & Hollis 1983), was detected in IC 860, NGC 4418, NGC 253 and NGC 4945. The line luminosity of CH_3CN 9-8 shows at least an order of magnitude higher values for NGC 4418 (L_{CH_3OH} = $1.66 \times 10^5 L_\odot$) and IC 860 ($2.37 \times 10^5 L_\odot$) than for NGC 253 ($6.36 \times 10^3 L_\odot$) and NGC 4945 ($2.52 \times 10^4 L_\odot$).

It seems likely that the CH_3CN emission is enhanced because of the high density and temperature in the CONs. The luminous CH_3CN emission in NGC 4418 may imply that the H_2S enhancement here is caused by desorption driven by radiation (Sec. 4.1.2), for example through UV radiation from a buried source. However, NGC 4418 has an extremely large H_2 column density with $N(H_2)$> 10^{25} cm^{-2} (Costagliola et al. 2013; Sakamoto et al. 2013). Since UV photons cannot penetrate long distances through such a high column density region, the global H_2S enhancement is unlikely to be caused by photodesorption by UV radiation. In addition, Bayet et al. (2009) argued that H_2S is unlikely to trace gas in Photon Dominated Regions (PDRs) in starburst galaxies, or near AGNs.

Alternatively, high energy photons and particles can pass through high column density cores and may photo- or thermally desorb H_2S out from grain surface over wider regions. Observations with the Chandra X-ray satellite by Maiolino et al. (2003) do not show a clear X-ray signature in NGC 4418. The extreme column densities of NGC 4418 are difficult to penetrate completely for X-rays. However, the X-rays reach further than UV and it is possible that they may impact the nuclear chemistry and provide large bulk gas temperatures that can result in an H_2S enhancement . González-Alfonso et al. (2013) proposed that X-ray ionisation due to an AGN is responsible for the molecular ion chemistry in the centre of NGC 4418.

Of the four LIRGs that have elevated H_2S/HCN intensity ratios, one does not show any evidence of either a molecular outflow or a "hot core": NGC 4826. This galaxy shows strong evidence of counter-rotating gas and stars, and its inner 1 kpc show the signatures of different types of m=1 perturbations (such as streaming motions) in the gas (García-Burillo et al. 2003). A possibility is that the perturbations drive turbulence that may also lead to H_2S enhancements (Sec. 4.1.1).

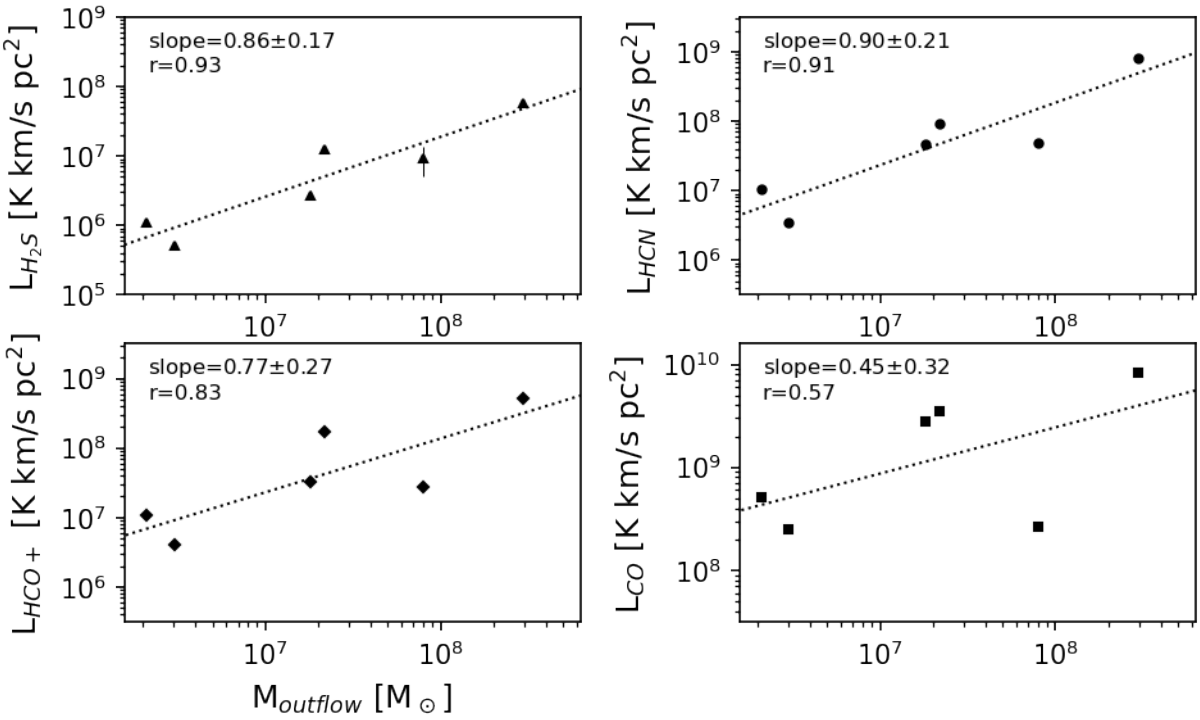

Fig. 4: Line luminosities of H_2S (top left), HCN (top right) and HCO^+ (lower left) 2–1, and CO 1–0 (lower right), of Circinus, NGC 3256, NGC 1068, NGC 253, NGC 4418 and Mrk 231 are plotted against the molecular mass of the outflow, $M_{\rm outflow}$, taken from Fluetsch et al. (2019). The correlation coefficient between the line luminosity and $M_{\rm out}$ is given in the upper left corner of each panel. Here, also the slope of the line is given.

4.5. Mass outflow rates and the global dense gas properties

In Sec. 4.3.1 we find no link between global H_2S abundance enhancements in the dense gas, and the presence (or velocity) of an outflow. There appears to be no general process that leads to significant H_2S abundance enhancements within the outflows, or when outflows are impacting their host galaxies. (Although enhancements are still possible on smaller scales that are diluted in our single dish beam.)

However, to understand the launch mechanism and outflow evolution, it is also important to study and compare other molecular properties of the host galaxy to that of its outflow. A correlation between the outflow mass, or its velocity, with for example the molecular gas mass or dense gas content of the host galaxy, gives essential clues to the origin of the molecular gas in the outflow.

To search for such host galaxy-outflow relations, we investigated correlations between the global line luminosity of H_2S, HCN, HCO^+ and the mass of the global molecular gas for our sample galaxies and the velocities and molecular masses of their outflows (Fluetsch et al. 2019, Table 2). The galaxies which are in our sample and also have their outflow information are Circinus, NGC 3256, NGC 1068, NGC 253, NGC 4418 and Mrk 231.

We find a correlation between $L(H_2S)$ and the molecular mass, $M_{\rm outflow}(H_2)$, of the outflow (Fig.4), where $L(H_2S)$ is highest for the galaxies with the highest $M_{\rm outflow}(H_2)$. This could be because $L(H_2S)$ is a rough probe of the host galaxy molecular mass and that the two are connected, i.e. that the ejected molecular gas mass is directly drawn from the large-scale molecular reservoir of the galaxy. This notion can be tested through investigating the correlation between $M_{\rm outflow}$ and other tracers of host galaxy molecular mass, such as the CO 1–0 luminosity, L(CO).

We use global CO 1—0 luminosities, (Sanders et al. 1991; Planesas et al. 1384; Aalto et al. 1995; Elmouttie et al. 1998; Houghton et al. 1997) for our sample galaxies, and find that L(CO) correlates more poorly with $M_{\rm outflow}(H_2)$ than $L(H_2S)$: the correlation coefficient is r=0.93 for H2S and r=0.57 for CO. : the correlation coefficient is r=0.93 for H_2S and r=0.50 for CO. The corresponding correlation coefficients for L(HCN) and $L(HCO^+)$ are r=0.91 and r=0.83, respectively. If we compare the critical densities, $n_{\rm crit}$, of the observed transitions, we find that H_2S and HCN have the highest $n_{\rm crit}$ followed by HCO^+ while the 1–0 transition of CO has an $n_{\rm crit}$ several orders of magnitude lower. *The molecular mass in the outflow appears to be more strongly connected to the dense gas (traced by H_2S and HCN) in the host galaxy, rather than the total available molecular reservoir.* Note that this suggested correlation between H_2S (and HCN) and the outflow mass, is different from the lack of correlation between H_2S abundances and outflow properties discussed in Sec 4.3. Here we use H_2S as a probe of the densest molecular gas, instead of searching for enhancements in the H_2S abundances as an effect of the outflow.

Since the correlations are found for the relatively limited number of sources in our sample, we decided to search for HCN data in the literature to test the notion that $M_{\rm outflow}(H_2)$ is more strongly correlated with the dense gas tracers than CO 1–0. We found HCN 1–0 data for 24 galaxies in the Fluetsch et al. (2019) sample (listed in table 6). HCN 1—0 has a lower critical density than the 2—1 transition and we expect to see a lower correlation coefficient with $M_{\rm outflow}(H_2)$ than for HCN 2—1, which we also find with a value of r=0.68 (Fig.5). Fluetsch et al. (2019)

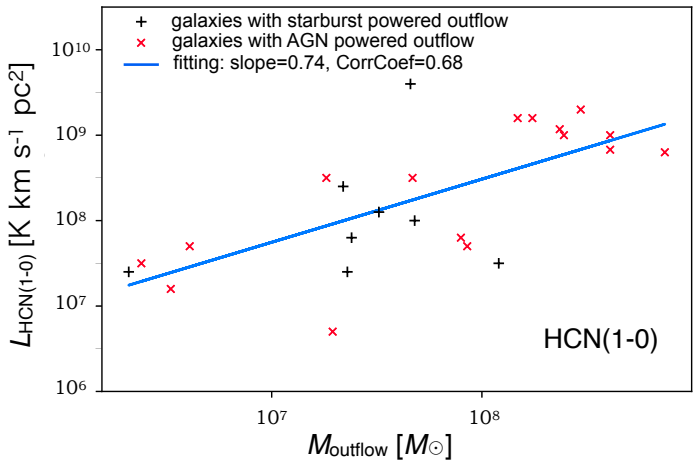

Fig. 5: Same plot as Fig.4 of the luminosities of HCN 1–0. The values for the molecular mass of the outflow, $M_{outflow}$, are from Fluetsch et al. (2019). L_{HCN1-0} are from the references in Table 6. AGN powered outflows are indicated with the red symbol x.

also lists values for $M(H_2)$ for their sample outflow host galaxies. Using these values for the 24 galaxies for which we have HCN 1—0 information, we find a correlation coefficient between $M(H_2)$ and $M_{outflow}(H_2)$ of r=0.25. This is significantly lower than what we find for L(CO) for our sample galaxies (Fig. 4). This may be because the molecular masses listed in (Fluetsch et al. 2019) are not global, masses, or because the the correlation between $M_{outflow}(H_2)$ and the total reservoir becomes even poorer in large samples.

A possible interpretation is that the molecular mass in the outflow is linked to the properties and mass of the most centrally concentrated gas, traced by HCN and H_2S. This is expected if the outflows are launched from the inner regions of galaxies. In addition, it also compatible with the scenario where the gas is being ejected from the host galaxy in molecular form (through entrainment by jets and winds, a molecular MHC (Magneto Hydrodynamic) wind, or by radiation pressure (e.g Veilleux et al. 2013)). It appears less consistent with the notion that the molecular gas is primarily formed in the outflows themselves through instabilities in the hot gas (e.g. Zubovas & King 2014; Ferrara & Scannapieco 2016).

Lutz et al. (2020) find a correlation between bolometric luminosity, L(bol), and $M_{outflow}(H_2)$, with similar relations that we find between L(HCN) and $M_{outflow}(H_2)$. They also find that the AGN luminosity, L(AGN), correlates with $M_{outflow}(H_2)$ for objects with L(AGN)>10^{10} $L_\odot$. Lutz et al. (2020) point out that L(bol) is linked to both AGN activity and star formation, making the relation to L(bol) somewhat difficult to interpret, but that AGN activity plays and important role in outflow driving. We note that the link between L(HCN) and $M_{outflow}(H_2)$ is stronger for the objects that Fluetsch et al. (2019) identify as AGN powered (see Fig. 5).

The correlation between $M_{outflow}$ and luminosity of dense gas tracers in the host galaxy should be tested on larger samples. Furthermore, high resolution imaging is required to test the notion of a higher degree of central concentration for H_2S and HCN and to what degree this emission is linked to the launch regions of outflows.

Table 6: HCN 1-0 data from the literature

Source	Log(M_{out}) [$M_\odot$]	Log(L_{HCN}) [K km s^{-1} pc^2]	Reference
IRAS F08572+3915	8.61	8.83	(1)
IRAS F10565+2448	8.37	9.07	(2)
IRAS 23365+3604	8.17	9.2	(2)
Mrk 273	8.24	9.2	(2)
I Zw 1	7.67	8.5	(3)
Mrk 231	8.47	9.3	(4)
NGC 1266	7.93	7.7	(2)
M82	8.08	7.5	(5)
NGC 1377	7.29	6.7	(2)
NGC 6240	8.61	9.0	(4)
NGC 3256	7.34	8.4	(2)
NGC 3628	7.36	7.4	(2)
NGC 253	6.32	7.4	(2)
NGC 6764	6.53	7.2	(6)
NGC 1068	7.26	8.5	(2)
NGC 2146	7.68	8.0	(2)
IRAS 17208-0014	7.66	9.6	(4)
NGC 1614	7.51	8.1	(5)
Circinus Galaxy	6.38	7.5	(7)
NGC 1808	7.38	7.8	(7)
M51	6.61	7.7	(5)
PG 0157 + 001	8.39	9.0	(3)
IRAS 05189-2524	8.87	8.8	(5)
NGC 4418	7.90	7.8	(8)

Notes. References:The mass of the outflow are taken from Table 2 of Fluetsch et al. (2019). The line luminosity:(1)Imanishi et al. (2007), (2)Huang et al. (2018), (3)Evans et al. (2006), (4)Gracia-Carpio et al. (2006), (5)Gao & Solomon (2004), (6)Contini et al. (1997), (7)Curran et al. (1999), (8)Costagliola et al. (2011)

4.6. H_2S and H_2O

Because of its chemical similarity, H_2S shares similar formation processes as H_2O, including the grain chemistry where both molecules may go through thermal- or photo- (non-thermal) desorption by shock or radiation. Although the more volatile H_2S will leave the grains at lower temperatures than more tightly bound H_2O (Rodgers & Charnley 2003). The discussion below is under two assumptions: 1) sulphur hydrogenates in H_2S on the dust grains, which is still debated, and 2) H_2S does not get dissociated when it is desorbed, even though Oba et al. (2019) showed it actually does. Due to the similarities it is conceivable that H_2S may serve as a water proxy, with its ground-state line accessible by ground-based telescopes for nearby galaxies. In this case, we would expect a correlation between the H_2O and H_2S properties of our sample galaxies and open up the possibility to use H_2S as an initial substitute in searches for water in nearby galaxies.

Yang et al. (2013) fitted several transition of water emission luminosities against the corresponding L_{IR} (see Yang et al. 2013, Fig. 1 and Table 1). The fit can be described as,

$$logL_{H_2O} = \alpha logL_{IR} + \beta. \quad (1)$$

They reported the results for eight transitions and the factor α varied between 0.78 and 1.21. For the ground state (para) H_2O line they find a α=0.89±0.09 (using χ^2 fitting). We carried out the same fitting for H_2S and HCN. The line luminosities were

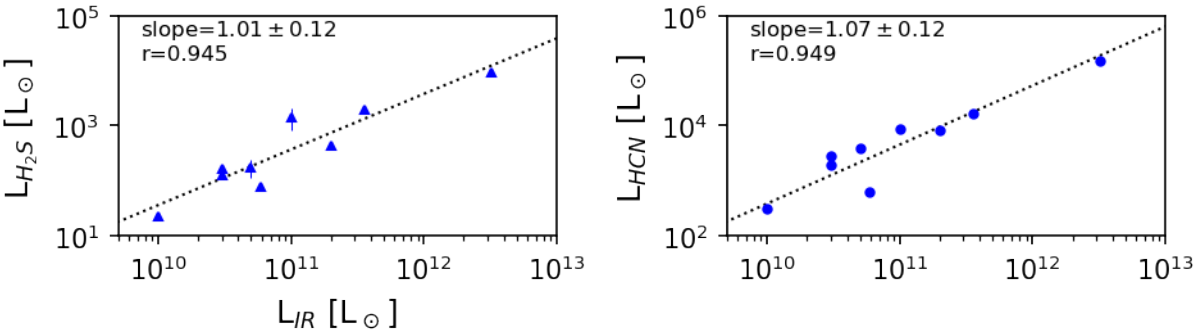

Fig. 6: Line Luminosity of H_2S (left) and HCN (right) versus Infrared luminosity of each sample galaxy in which H_2S line is detected. The correlation coefficient and the slope of the fitting line are given in the upper left corner of each panel.

calculated using the formula $L_{\rm line}[L_\odot] = 1.04\times10^{-3}\times S_{\rm line}\Delta v D_{\rm L}^2\times \nu_{\rm obs}$, where $S_{\rm line}\Delta v$ is the measured flux of the line [Jy km s^{-1}], $D_{\rm L}$ is the luminosity distance [Mpc] and$\nu_{\rm obs}$ is the frequency of the line [GHz]. I[Jy km s^{-1}] = I[K km s^{-1}] × 40.67 [Jy K^{-1}] is used to calculate the line flux from the observed antenna temperature (Carilli & Walter 2013)[6]. In Fig. 6 we show plots of the line luminosity of H_2S and HCN versus the infrared luminosity of each galaxy.

We found a factor α (in the Eq.(1)) of 1.01±0.12 (χ^2) for H_2S and 1.07±0.12 (χ^2) for HCN. This is within the error of the value found for the ground-state H_2O line. Yang et al. (2013) suggested that the reason that the correlation between H_2O and IR is near-linear is IR pumping of the H_2O lines. They argue that, after absorbing a far-IR photon, the upper levels cascade down to populate lower levels in a constant fraction, yielding a linear relationship with $L_{\rm IR}$, and that the linear correlation shows the importance of IR-pumping. Although it is true that IR-pumping is important for the excitation of H_2O it is not clear that the same logic can be applied to the near-linear correlations found for H_2S and HCN. Crockett et al. (2014) claim that IR pumping of H_2S for transitions lower than J=3 is not possible. The near-linear correlation between $L_{\rm HCN}$ and $L_{\rm IR}$ (first reported for LIRGs by (Gao & Solomon 2004)) is also not clearly connected to IR pumping (even if the HCN rotational ladder can be pumped via a mid-IR bending mode (e.g. Aalto et al. 1994)). Gao & Solomon (2004) argue that the HCN-IR correlation is due to HCN probing dense gas engaged in star formation, that in turn gives rise to the IR luminosity. We conclude that H_2S, H_2O and HCN seem to correlate in a similar way with $L_{\rm IR}$ which may indicate that they emerge from similar regions in the LIRGs.

5. Conclusions

Using the APEX telescope, we observed the λ=2 mm 1_{10}–1_{01} line of ortho-H_2S towards the centres of 12 nearby luminous galaxies and detected H_2S emission in nine of them. We also detected HCN and HCO^+ 2–1 in 11 of the sample galaxies and also HNC, SO, CH_3OH, CH_3CN, H_2CS and HOC^+ in some galaxies. In addition, we observed H_2S in the ULIRG Mrk 231 with the NOEMA telescope. Our aim was to study the impact of outflows on the chemistry and physical conditions of the gas in the host galaxy and outflow, using H_2S as a potential tracer of the impact of shocks. The line intensity ratio of H_2S to HCN (and to HCO^+) shows considerable variation, which could be due to significant changes of H_2S abundance among the studied galaxies. Four galaxies stand out to be particularly H_2S luminous: two of them exhibiting strong outflows, one harbouring a Compact Obscured Nucleus (CON) and one shows evidence of gas and star counter-rotation possibly feeding turbulence. These results support previous suggestions that the H_2S emission may become enhanced in both shocked and irradiated dusty gas in the centres of luminous, gas-rich galaxies. However, for the sample galaxies as a whole, we find no correlation between the H_2S/HCN or the H_2S/HCO^+ line ratios with the presence of a molecular outflow or its speed. In Mrk 231 we detect H_2S out to -300 and +500 kms^{-1}, but the emission is not enhanced with respect to that of HCN. The relatively faint H_2S emission in the line wings appears inconsistent with the notion of shock-chemistry in the molecular outflow of Mrk 231.

We also investigated other possible connections between host galaxy molecular properties and that of their outflows. We found no link between the luminosities of H_2S 1_{10}–1_{01} , HCN 2–1 , HCO^+2–1 or CO 1–0 with the outflow velocity. In contrast, we did find a correlation with the molecular mass of the outflow, $M_{\rm outflow}(H_2)$, where the correlation coefficient is strongest for $L_{\rm H_2S}$ and $L_{\rm HCN}$ and weakest for $L_{\rm CO}$. We suggest that $L_{\rm H_2S}$ serves as a tracer of the dense gas content, similar to $L_{\rm HCN}$, and that the correlation between $L_{\rm H_2S}$ and $M_{\rm outflow}(H_2)$ implies a relation between the dense gas reservoir and the properties and evolution of the molecular feedback. The dense gas component is likely more centrally concentrated than the bulk of the molecular gas (traced by CO 1–0) and a possible explanation is that the outflows are launched in the central regions and that the molecular gas in the outflow stems from the reservoir in the inner region, rather than being formed from instabilities in the hot gas. However, further studies of this correlation is important to understand its cause. In addition, it is important to mention that the enhancement of H_2S could also be related to starburst regions dominated by dense molecular gas and UV radiation.

Finally, based on chemical similarities between H_2S and H_2O, we studied if the two species show analogous behaviour in how they correlate to the IR luminosity. We find that their IR-correlation coefficients are similar that could indicate that they originate in the same regions in the galaxy: warm gas in shocks or irradiated by star formation or an AGN.

Acknowledgements. This research has made use of the services of the ESO Science Archive Facility. Based on observations collected at the European Organisation for Astronomical Research in the Southern Hemisphere under ESO programmes 096.F-9331(A), 099.F-9312(A) and 0100.F-9311(A). Based on observations with the APEX telescope. APEX is a collaboration between the Max-Planck-Institut für Radioastronomie, the European Southern Observatory,

[6] http://www.apex-telescope.org/telescope/efficiency/index.php?yearBy=2017

and the Onsala Observatory. Based on observations carried out under project number W16BW with the IRAM NOEMA Interferometer. IRAM is supported by INSU/CNRS (France), MPG (Germany) and IGN (Spain). M.S., S.A. and S.K. gratefully acknowledges funding from the European Research Council (ERC) under the European Union's Horizon 2020 research and innovation programme (grant agreement No 789410) SV acknowledges the European Research Council (ERC) Advanced Grant MOPPEX 833460. YN is supported by NAOJ ALMA Scientific Research grant No. 2017-06B and JSPS KAKENHI grant No. JP18K13577.

References

Aalto, S. 2012, Proceedings of the International Astronomical Union, 8, 199
Aalto, S., Booth, R. S., Black, J. H., & Johansson, L. E. 1995, Astronomy & Astrophysics, 300, 369A
Aalto, S., Booth, R. S., Black, J. H., Koribalski, B., & Wielebinski, R. 1994, Astronomy & Astrophysics, 286, 365
Aalto, S., Costagliola, F., Muller, S., et al. 2016, Astronomy and Astrophysics, 590
Aalto, S., Falstad, N., Muller, S., et al. 2020, Astronomy & Astrophysics, 1
Aalto, S., Garcia-Burillo, S., Muller, S., et al. 2015a, Astronomy & Astrophysics, 574, A85
Aalto, S., Garcia-Burillo, S., Muller, S., et al. 2012, Astronomy and Astrophysics, 537, 1
Aalto, S., Martin, S., Costagliola, F., et al. 2015b, Astronomy and Astrophysics, 584
Aalto, S., Muller, S., König, S., et al. 2019, Astronomy and Astrophysics, 627
Barbosa, F. K. B., Storchi-Bergmann, T., Mcgregor, P., Vale, T. B., & Rogemar Riffel, A. 2014, Monthly Notices of the Royal Astronomical Society, 445, 2353
Barcos-Muñoz, L., Aalto, S., Thompson, T. A., et al. 2018, The Astrophysical Journal, 853, L28
Bayet, E., Viti, S., Williams, D. A., Rawlings, J. M., & Bell, T. 2009, Astrophysical Journal, 696, 1466
Blake, G. A., Sutton, E. C., Masson, C. R., & Phillips, T. G. 1987, The Astrophysical Journal, 315, 621
Bolatto, A. D., Warren, S. R., Leroy, A. K., et al. 2013a, Nature, 499, 450
Bolatto, A. D., Wolfire, M., & Leroy, A. K. 2013b, Annual Review of Astronomy and Astrophysics, 51, 207
Brauher, J. R., Dale, D. A., & Helou, G. 2008, The Astrophysical Journal Supplement Series, 178, 280
Carilli, C. & Walter, F. 2013, Annual Review of Astronomy and Astrophysics, 51, 105
Charnley, S. B. 1997, The Astrophysical Journal, 481, 396
Chung, A., Yun, M. S., Naraynan, G., Heyer, M., & Erickson, N. R. 2011, Astrophysical Journal Letters, 732, 1
Churchwell, E. & Hollis, J. 1983, The Astrophysical Journal, 272, 591
Cicone, C., Maiolino, R., Aalto, S., Muller, S., & Feruglio, C. 2020, Astronomy & Astrophysics, 633, A163
Cicone, C., Maiolino, R., Sturm, E., et al. 2014, Astronomy and Astrophysics, 562, 1
Contini, T., Wozniak, H., Considère, S., & Davoust, E. 1997, Astronomy and Astrophysics, 324, 41
Costagliola, F., Aalto, S., Rodriguez, M. I., et al. 2011, Astronomy and Astrophysics, 528, 1
Costagliola, F., Aalto, S., Sakamoto, K., et al. 2013, Astronomy and Astrophysics, 556
Costagliola, F., Sakamoto, K., Muller, S., et al. 2015, Astronomy and Astrophysics, 582, 1
Crockett, N. R., Bergin, E. A., Neill, J. L., et al. 2014, Astrophysical Journal, 781
Curran, S. J., Rydbeck, G., Johansson, L. E. B., & Booth, R. S. 1999, October, 778, 767
Dasyra, K. M., Combes, F., Oosterloo, T., et al. 2016, Astronomy and Astrophysics, 595, 2
Elmouttie, M., Krause, M., Haynes, R. F., & Jones, K. L. 1998, Monthly Notices of the Royal Astronomical Society, 300, 1119
Emsellem, E., Fathi, K., Wozniak, H., et al. 2006, Monthly Notices of the Royal Astronomical Society, 365, 367
Esplugues, G. B., Viti, S., Goicoechea, J. R., & Cernicharo, J. 2014, Astronomy and Astrophysics, 567, 1
Evans, A., Solomon, P., Tacconi, L., Vavilkin, T., & Downes, D. 2006, The Astronomical Journal, 132, 2398
Falstad, N., Hallqvist, F., Aalto, S., et al. 2019, Astronomy and Astrophysics, 623
Ferrara, A. & Scannapieco, E. 2016, The Astrophysical Journal, 833, 46
Feruglio, C., Daddi, E., Fiore, F., et al. 2011, Astrophysical Journal Letters, 729, 2
Feruglio, C., Maiolino, R., Piconcelli, E., et al. 2010, Astronomy and Astrophysics, 518, 1
Fluetsch, A., Maiolino, R., Carniani, S., et al. 2019, Monthly Notices of the Royal Astronomical Society, 483, 4586
Gao, Y. & Solomon, P. M. 2004, The Astrophysical Journal, 606, 271
García-Burillo, S., Combes, F., Hunt, L. K., et al. 2003, Astronomy and Astrophysics, 407, 485
García-Burillo, S., Combes, F., Usero, A., et al. 2015, Astronomy and Astrophysics, 580, 1
García-Burillo, S., Combes, F., Usero, A., et al. 2014, Astronomy and Astrophysics, 567, 1
Gerin, M., Nakai, N., & Combes, F. 1988, Astronomy and Astrophysics, 203, 44
Goicoechea, J. R., Aguado, A., Cuadrado, S., et al. 2021, Astronomy & Astrophysics, 647, A10
González-Alfonso, E., Fischer, J., Bruderer, S., et al. 2013, Astronomy & Astrophysics, 550, A25
González-Alfonso, E., Fischer, J., Graciá-Carpio, J., et al. 2012, Astronomy and Astrophysics, 541
González-Alfonso, E., Fischer, J., Isaak, K., et al. 2010, Astronomy and Astrophysics, 518, 10
Gracia-Carpio, J., Garcia-Burillo, S., Planesas, P., & Colina, L. 2006, 135
Heikkilä, A., Johansson, L. E., & Olofsson, H. 1999, Astronomy and Astrophysics, 344, 817
Henkel, C., Mühle, S., Bendo, G., et al. 2018, Astronomy and Astrophysics, 615, 1
Holdship, J., Viti, S., Makrymallis, A., & Priestley, F. 2017, The Astronomical Journal, 154, 38
Houghton, S., Whiteoak, J. B., Koribalski, B., et al. 1997, Astronomy and Astrophysics, 325, 923
Huang, Y., Zhang, J. S., Liu, W., & Xu, J. 2018, Journal of Astrophysics and Astronomy, 39
Imanishi, M., Nakanishi, K., Tamura, Y., Oi, N., & Kohno, K. 2007, The Astronomical Journal, 134, 2366
Iono, D., Wilson, C. D., Yun, M. S., et al. 2009, Astrophysical Journal, 695, 1537
Israel, F. P., Güsten, R., Meijerink, R., Requena-Torres, M. A., & Stutzki, J. 2017, Astronomy and Astrophysics, 599, 1
Klessen, R. S. & Glover, S. C. O. 2016, 85
Lindberg, J. E., Aalto, S., Muller, S., et al. 2016, Astronomy and Astrophysics, 587, 1
Lucas, R. & Liszt, H. S. 2002, Astronomy & Astrophysics, 384, 1054
Lutz, D., Sturm, E., Janssen, A., et al. 2020, Astronomy & Astrophysics, 633, A134
Maiolino, R., Comastri, A., Gilli, R., et al. 2003, Monthly Notices of the Royal Astronomical Society, 344, L59
Maiolino, R., Russell, H. R., Fabian, A. C., et al. 2017, Nature, 544, 202
Mangum, J. G., Darling, J., Henkel, C., et al. 2013, Astrophysical Journal, 779
Mangum, J. G., Ginsburg, A. G., Henkel, C., et al. 2019, The Astrophysical Journal, 871, 170
Mangum, J. G. & Shirley, Y. L. 2015, Publications of the Astronomical Society of the Pacific, 127, 266
Mangum, J. G. & Shirley, Y. L. 2016, Publications of the Astronomical Society of the Pacific, 128, 029201
Mangum, J. G. & Shirley, Y. L. 2017, Publications of the Astronomical Society of the Pacific, 129, 069201
Martín, S., Krips, M., Aalto, S., et al. 2011, 36
Martin, S., Martin-Pintado, J., Mauersberger, R., Henkel, C., & Garcia-Burillo, S. 2005, The Astrophysical Journal, 620, 210
Matsushita, S., Trung, D.-V., Boone, F., et al. 2015, Publications of The Korean Astronomical Society, 30, 439
Michiyama, T., Iono, D., Sliwa, K., et al. 2018, The Astrophysical Journal, 868, 95
Minh, Y. C., Irvine, W. M., McGonagle, D., & Ziurys, L. M. 1990, The Astrophysical Journal, 360, 136
Minh, Y. C., Muller, S., Liu, S.-Y., & Yoon, T. S. 2007, The Astrophysical Journal, 661, L135
Mitchell, G. F. 1984, The Astrophysical Journal, 287, 665
Morganti, R., Oosterloo, T., Raymond Oonk, J. B., Frieswijk, W., & Tadhunter, C. 2015, Astronomy and Astrophysics, 580
Navarro-Almaida, D., Gal, R. L., Fuente, A., et al. 2020, Astronomy & Astrophysics, 39, A39
Nishimura, Y., Watanabe, Y., Harada, N., et al. 2017, The Astrophysical Journal, 848, 17
Oba, Y., Tomaru, T., Kouchi, A., & Watanabe, N. 2019, The Astrophysical Journal, 874, 124
Ohyama, Y., Sakamoto, K., Aalto, S., & III, J. S. G. 2019, The Astrophysical Journal, 871, 191

Pereira-Santaella, M., Colina, L., García-Burillo, S., et al. 2018, Astronomy and Astrophysics, 616, 1
Pineau des Forets, G., Roueff, E., Schilke, P., & Flower, D. R. 1993, Monthly Notices of the Royal Astronomical Society, 262, 915
Planesas, P., Gómez-González, J., & Martín-Pintado, J. 1384
Privon, G. C., Herrero-Illana, R., Evans, A. S., et al. 2015, Astrophysical Journal, 814
Rodgers, S. D. & Charnley, S. B. 2003, The Astrophysical Journal, 585, 355
Sakamoto, K., Aalto, S., Barcos-Muñoz, L., et al. 2017, The Astrophysical Journal, 849, 14
Sakamoto, K., Aalto, S., Combes, F., Evans, A., & Peck, A. 2014, Astrophysical Journal, 797
Sakamoto, K., Aalto, S., Costagliola, F., et al. 2013, Astrophysical Journal, 764
Salak, D., Nakai, N., & Kitamoto, S. 2014, Publications of the Astronomical Society of Japan, 66, 1
Sanders, D. B., Mazzarella, J. M., Kim, D.-C., Surace, J. A., & Soifer, B. T. 2003, The Astronomical Journal, 126, 1607
Sanders, D. B. & Mirabel, I. F. 1996, 749
Sanders, D. B., Scoville, N. Z., & Soifer, B. T. 1991, The Astrophysical Journal, 370, 158
Shirley, Y. L. 2015, Publications of the Astronomical Society of the Pacific, 127, 299
Spoon, H. W., Farrah, D., Lebouteiller, V., et al. 2013, Astrophysical Journal, 775
Sturm, E., Gonzlez-Alfonso, E., Veilleux, S., et al. 2011, Astrophysical Journal Letters, 733
Veilleux, S., Maiolino, R., Bolatto, A. D., & Aalto, S. 2020, Astronomy and Astrophysics Review, 28
Veilleux, S., Meléndez, M., Sturm, E., et al. 2013, Astrophysical Journal, 776
Viti, S., Collings, M. P., Dever, J. W., McCoustra, M. R., & Williams, D. A. 2004, Monthly Notices of the Royal Astronomical Society, 354, 1141
Wakelam, V., Castets, A., Ceccarelli, C., et al. 2004, Astronomy and Astrophysics, 413, 609
Walter, F., Bolatto, A. D., Leroy, A. K., et al. 2017, The Astrophysical Journal, 835, 265
Woods, P. M., Occhiogrosso, A., Viti, S., et al. 2015, Monthly Notices of the Royal Astronomical Society, 450, 1256
Yang, C., Gao, Y., Omont, A., et al. 2013, Astrophysical Journal Letters, 771
Zschaechner, L. K., Walter, F., Bolatto, A., et al. 2016, The Astrophysical Journal, 832, 1
Zubovas, K. & King, A. R. 2014, Monthly Notices of the Royal Astronomical Society, 439, 400

Appendix A: Spectra of the APEX sample galaxies.

Appendix B: APEX results

Appendix C: Notes on Critical Densities

In this paper, the critical densities of H_2S, HCN and HCO^+ were calculated assuming the molecules are two-level systems,

$$n_{crit} = A_{ul}/q_{ul} \tag{C.1}$$

where A_{ul} is the spontaneous transition probability of the transition u to l and q_{ul} is the corresponding collisional rate coefficient. This simple approach is sufficient for the comparison of critical densities in Sec.4.2.

A more realistic estimate of the critical density is,

$$n_{crit} = A_{ul}/(\sum_{l<u} q_{ul} + \sum_{u'>u} q_{uu'}) \tag{C.2}$$

where one allows for transitions between more levels. In general it gives lower values. Furthermore, opacity will also impact the critical density. For further discussion, see for example Shirley (2015).

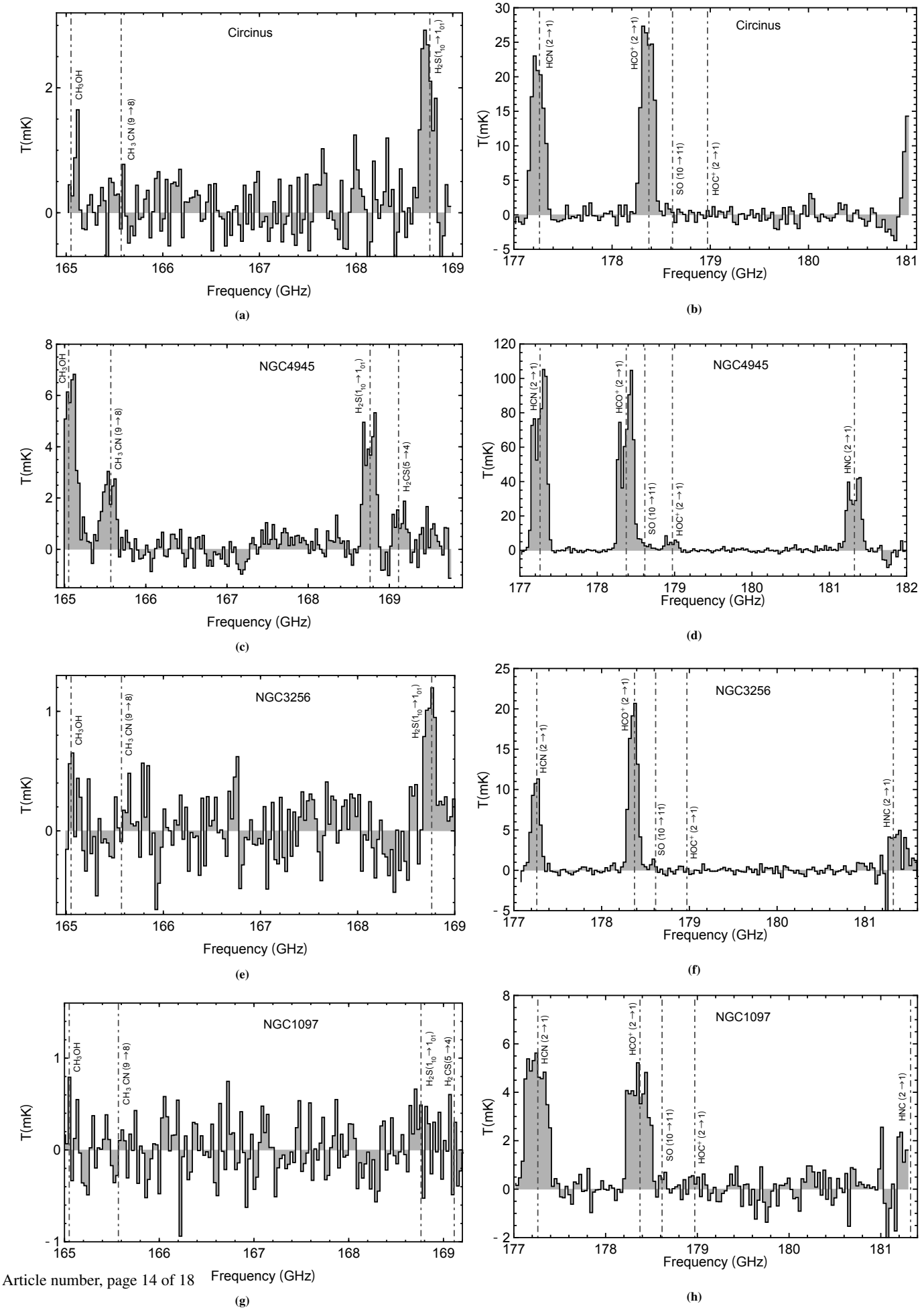

Fig. A.1: Spectra taken with SEPIA. The intensity scale is in T_A^*, not corrected for the beam efficiency, which at this frequencies is 0.78.

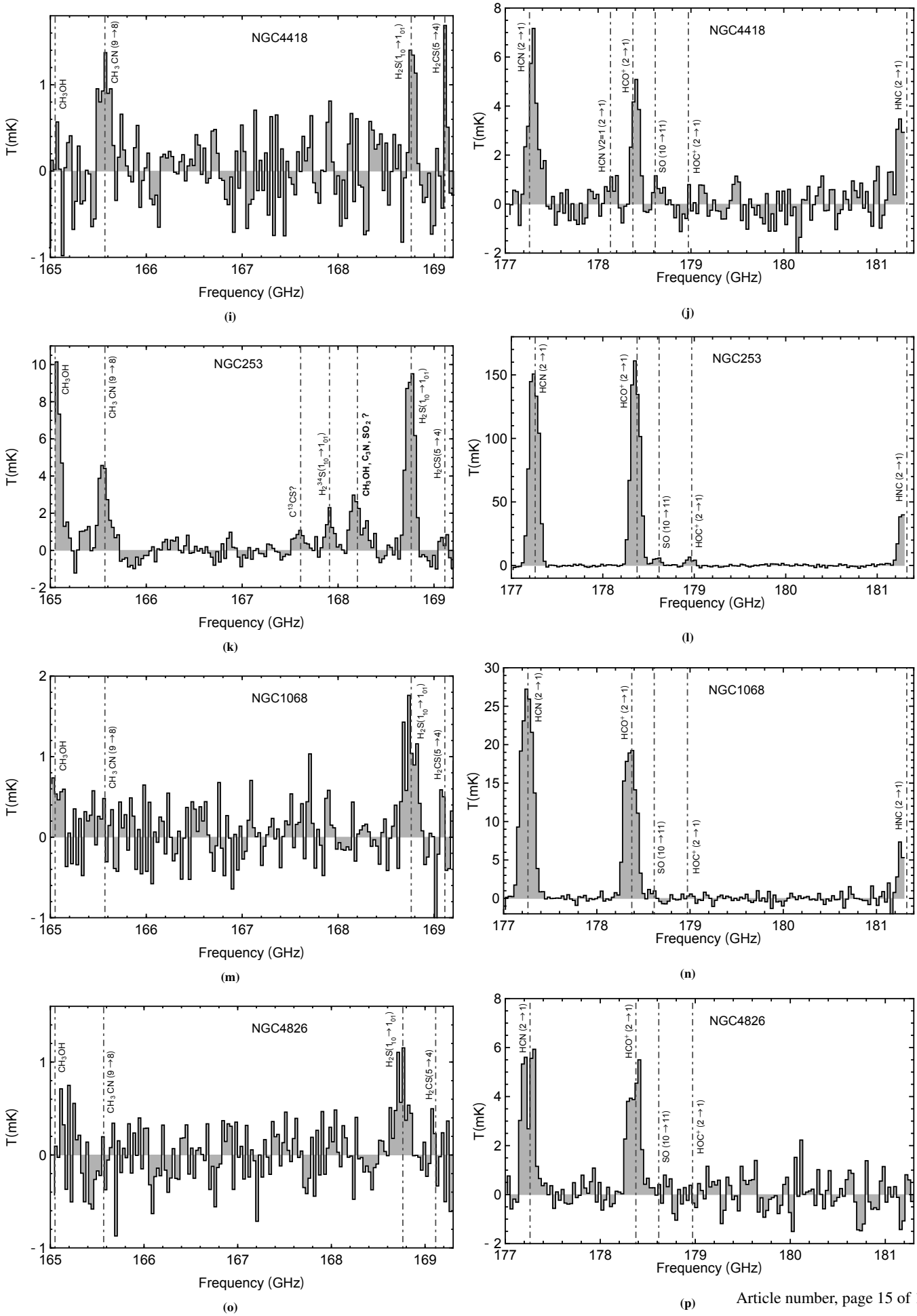

Fig. A.1: (continued)

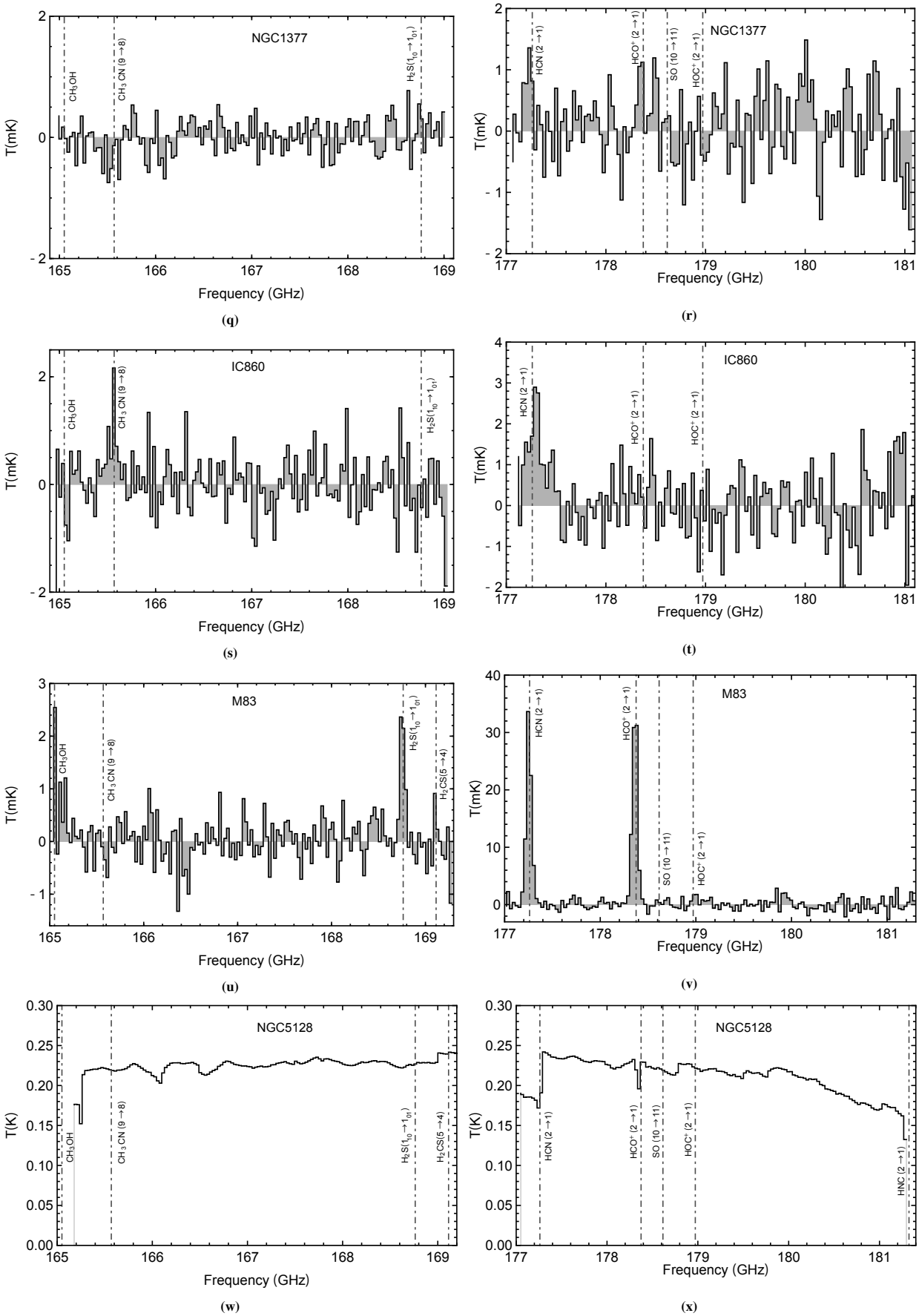

Fig. A.1: (continued)

Table B.1: APEX results

Source	Molecule	Line peak ($T_{A,peak}$)[b] (mK)	I (K kms^{-1})	Δv (kms^{-1}))	rms (mK)
NGC 3256	CH_3OH	>2.1±0.2	>0.06±0.03	238±43	0.20
	H_2S	1.2±0.7	0.28±0.03	216±61	0.20
	HCN	16.9±0.4	2.26±0.06	182±7	0.38
	HCO^+	21.6±0.4	4.17±0.06	186±4	0.38
	SO	1.2±0.4	0.13±0.03	85±4	0.38
	HNC	4.4±2.0	>1.02±0.04	284±145	0.38
NGC 1068	CH_3OH	>0.7±0.2	>0.18±0.04	303±185	0.35
	H_2S	1.4±0.3	0.40±0.06	267±60	0.35
	HCN	28.4±0.6	7.41±0.10	253±6	0.60
	HCO^+	20.7±0.6	5.32±0.11	250±8	0.60
	SO	1.0±0.5	0.14±0.04	133±73	0.60
	HNC	7.6±0.9	>0.73±0.06	104±18	0.60
IC 860	CH_3CN	1.4±0.5	0.39±0.09	192±87	0.52
	HCN	2.2±0.3	0.82±0.15	357±63	0.80
NGC 4418	CH_3CN	1.3±0.3	0.27±0.11	216±56	0.41
	H_2S	1.6±0.4	0.25±0.11	126±39	0.41
	H_2CS	1.7±0.5	>0.11±0.03	—	0.41
	HCN	6.4±0.4	1.45±0.10	200±16	0.67
	HCO^+	5.3±0.5	0.84±0.08	151±15	0.67
	SO	0.9±0.5	0.18±0.07	166±15	0.67
	HNC	3.3±0.5	>0.70±0.07	251±103	0.67
Circinus	CH_3OH	>2.0±1.0	>0.16±0.04	63±37	0.37
	H_2S	3.0±0.4	0.78±0.06	241±33	0.37
	HCN	24.0±1.0	6.0±0.1	233±11	0.81
	HCO^+	29.5±1.0	7.0±0.1	238±9	0.81
	SO	4.2±1.0	0.16±0.08	38±9	0.81
	HNC	—	>0.93±0.08	—	0.81
NGC 1097	CH_3OH	>0.8±0.2	>0.04±0.04	18±273	0.30
	H_2S	0.5±0.3	0.11±0.04	157±89	0.30
	HCN	5.9±0.3	2.38±0.10	409±26	0.51
	HCO^+	4.9±0.3	1.97±0.09	405±29	0.51
	HNC	2.4±1.0	>0.33±0.05	126±63	0.51
NGC 4945	CH_3OH	7.2±1.1	>1.92±0.08	238±43	0.46
	CH_3CN	2.8±0.3	0.96±0.08	345±39	0.46
	H_2S	4.8±0.5	1.49±0.07	295±35	0.46
	H_2CS	1.4±0.5	0.46±0.07	275±38	0.46
	HCN	95.5±7.1	31.3±0.2	325±28	1.0
	HCO^+	85.6±5.4	30.1±0.2	337±25	1.0
	SO	—	0.24±0.16	—	1.0
	HOC^+	5.5±1.0	1.75±0.16	322±69	1.0
	HNC	38.3±2.8	13.3±0.2	339±28	1.0
NGC 253	CH_3OH	9.5±1.4	>1.93±0.07	183±45	0.48
	CH_3CN	4.7±1.0	1.05±0.08	208±35	0.48
	H_2S	10.4±1.1	3.09±0.06	187±24	0.48
	H_2CS	0.7±1.1	0.12±0.05	126±23	0.48
	HCN	161.4±3.7	33.5±0.14	203±5	0.87
	HCO^+	165.3±2.8	33.7±0.14	197±4	0.87
	SO	6.2±0.6	1.00±0.10	162±20	0.87
	HOC^+	6.1±0.9	1.03±0.11	157±27	0.87
	HNC	>42.9±0.8	>3.91±0.10	135±5	0.87
NGC 1377	HCN	1.3±0.4	0.76±0.1	135±45	0.60
M 83	CH_3OH	0.9±0.3	>0.29±0.03	377±242	0.51
	H_2S	2.6±0.4	0.31±0.05	107±19	0.51
	HCN	34.0±0.9	3.95±0.13	106±3	0.96
	HCO^+	36.0±0.9	4.21±0.13	108±3	0.96
	HOC^+	1.1±0.9	0.39±0.14	273±3	0.96
NGC 4826	H_2S	0.9±0.2	0.27±0.09	288±58	0.27
	HCN	5.5±0.6	1.54±0.11	273±31	0.66
	HCO^+	4.9±0.4	1.38±0.13	270±22	0.66

Table B.1: continued.

Source	Molecule	Line peak ($T_{\mathrm{A,peak}}$)^b (mK)	I (K kms^{-1})	Δv (kms^{-1}))	rms (mK)
NGC 5128	-	-	-	-	-

Notes. Integrated line intensities are calculated using the formula: $I_{\mathrm{line}} = \sum_{\mathrm{i}} I_{\mathrm{i}} dv$, where I is the intensity at each velocity and dv is the velocity resolution.The errors are calculated using,$\Delta I_{\mathrm{line}} = \sqrt{(\Delta I_{\mathrm{L}})^2 + (\Delta I_{\mathrm{B}})^2} = \sqrt{(\sigma v_{\mathrm{res}} \sqrt{N_{\mathrm{L}}})^2 + (\sigma v_{\mathrm{res}} N_{\mathrm{L}} / \sqrt{N_{\mathrm{B}}})^2}$, where σ is the rms, v_{res} is the velocity resolution, N_{L} is the number of channels that contribute to the line and N_{B} is the number of channels which is outside the line. The RMS noise levels are given in Table 1. NGC 5128 has strong continuum emission and its noise levels could not be measured.